JACS
JOURNAL OF THE AMERICAN CHEMICAL SOCIETY
Article
pubs.acs.org/JACS

Synthesis, Characterization, and Electrochemical Studies of $PPh_{3-n}(dipp)_n$ (dipp = 2,6-Diisopropylphenyl): Steric and Electronic Effects on the Chemical and Electrochemical Oxidation of a Homologous Series of Triarylphosphines and the Reactivities of the Corresponding Phosphoniumyl Radical Cations

John P. Bullock,*[,†] Alan M. Bond,*[,‡] René T. Boeré,*[,§] Twyla M. Gietz,[§] Tracey L. Roemmele,[§] Sonja D. Seagrave,[§] Jason D. Masuda,[∥] and Masood Parvez[⊥]

[†]Division of Natural Sciences & Mathematics, Bennington College, Bennington, Vermont 05201, United States

[‡]School of Chemistry, Monash University, Clayton, Victoria 3800, Australia

[§]Department of Chemistry and Biochemistry, University of Lethbridge, Lethbridge, AB, Canada T1K3M4

[∥]The Maritimes Centre for Green Chemistry and the Department of Chemistry, Saint Mary's University, Halifax, Nova Scotia, Canada B3H 3C3

[⊥]Department of Chemistry, University of Calgary, Calgary, AB, Canada T2N1N4

Supporting Information

ABSTRACT: Activation barriers to the electrochemical oxidation for the series $PPh_{3-n}(dipp)_n$ (dipp = 2,6-diisopropylphenyl) in CH_2Cl_2/Bu_4NPF_6 were measured using large amplitude FT ac voltammetry. Increasing substitution across this series, which offers the widest range of steric requirements across any analogous series of triarylphosphines reported to date, increases the energetic barrier to electron transfer; values of 18, 24, and 25 kJ mol^{-1} were found for compounds with n = 1, 2, and 3, respectively. These values are significantly greater than those calculated for outer sphere activation barriers, with deviations between observed and calculated values increasing with the number of dipp ligands. This suggests that the steric congestion afforded by these bulky substituents imposes significant reorganizational energy on the electron transfer processes. This is the first investigation of the effect of sterics on the kinetics of heterogeneous electron transfer across a structurally homologous series. Increased alkyl substitution across the series also increases the chemical reversibility of the oxidations and decreases the oxidation peak potentials. As the compounds for which n = 1 and 2 are novel, the synthetic strategies employed in their preparation are described, along with their full spectroscopic, physical, and crystallographic characterization. Optimal synthesis when n = 1 is via a Grignard reagent, whereas when n = 2 an aryl copper reagent must be employed, as use of a Grignard results in reductive coupling. Chemical oxidation studies were performed to augment the electrochemical work; the O, S, and Se oxidation products for the parent triarylphosphines for which n = 1 and 2 were isolated and characterized.

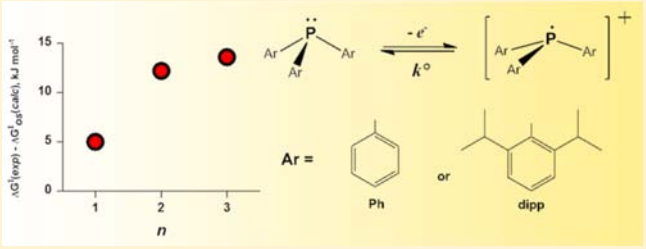

INTRODUCTION

The influence of sterics on chemical reactions has long been recognized. The kinetics and thermodynamics of organic[1a] and inorganic[1b] substitution, Lewis acid/base,[1c] and radical reaction pathways[1d] can all be strongly affected by the size of structural features of either the substrate or an attacking species. Redox reactions can likewise be influenced by sterics. Since any homogeneous electron transfer reaction requires appropriate orbital overlap between the donor and acceptor species, features that diminish such overlap will reduce the corresponding rate constants. Moreover, the operative mechanism for any particular redox reaction, i.e., the tendency to proceed via an inner or an outer sphere process, can depend on the steric interactions between donor and acceptor.[2] There is, however, a dearth of systematic studies concerning the influence of sterics on *heterogeneous* electron transfer processes. As part of our continuing study of sterically hindered phosphines, we undertook a study on the electrochemistry of $PPh_{3-n}(dipp)_n$ (Chart 1, dipp = 2,6-diisopropylphenyl); given the relative sizes of the Ph and dipp ligands, the title homologous series spans the entire known steric range of triarylphosphines. Using a powerful new implementation of large amplitude ac voltammetry,[3] we measured the activation energy of the electrode

Received: April 20, 2013
Published: June 28, 2013

   dx.doi.org/10.1021/ja403555d | J. Am. Chem. Soc. 2013, 135, 11205−11215

Chart 1

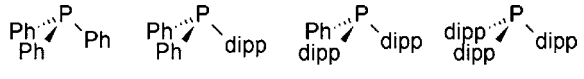

processes for complexes **1**, **2**, and **3** and found that the presence of the ortho isopropyl substituents systematically increases the activation barrier to oxidation. This represents, we believe, the first such systematic study that demonstrates the effect of steric crowding on the electrode processes across a series of structurally analogous compounds.

The unexpected effect of sterics on the heterogeneous electron transfer kinetics is not only interesting in its own right, it is also of obvious relevance to the burgeoning field of the steric modulation of reactions. Specifically, the use of bulky substituents is now recognized as essential for the stabilization and isolation of new modalities at the frontiers of chemistry, especially main-group element chemistry. Numerous examples can be cited: heavy element multiple bonds,[4a−d] bulky *N*-heterocyclic carbenes,[4e−j] isolation of low-coordinate molecules and radicals,[4k−m] heavy group 14 R_3E free radicals,[4n] and the first stable, isolable phosphanyl radical.[4o] Most recently, Pan and co-workers successfully used a combination of the bulky 2,4,6-triisopropylphenyl (tripp) group and superbulky weakly coordinating anions to crystallographically characterize P(tripp)$_3^{+\bullet}$ and [tripp$_2$PPtripp$_2$]$^{+\bullet}$, the first time phosphoniumyl radical cations have been so examined.[5] Protasiewicz and co-workers have drawn attention to unexpected consequences of sterically demanding substituents in phosphorus chemistry,[6] showing, *inter alia*, that the lengths of P═P bonds may be affected by crystal disorder induced by the packing demands of the bulky substituents.[6a] Finally, the work we describe herein is also relevant to recent efforts in the area of frustrated Lewis pairs, as the promising catalytic chemistry such systems exhibit often involves oxidation of an exceptionally hindered moiety.[7] The effects we describe may also be operative in such systems, thereby influencing the kinetics of the corresponding catalytic redox processes. We attribute the steric enhancement of the oxidative activation barrier to an increase in the reorganizational energy of the compounds associated with the electron transfer; the more enmeshed the alkyl groups are in the parent compound, the more energetically demanding is the reorganization.

As two of the compounds in the series, **1** and **2**, are novel, we also describe in this article the specific synthetic strategies employed in their preparation, as well as details of their physical and spectroscopic characterization, especially as they inform the interpretation of the kinetic studies. In addition, we performed a series of DFT calculations of the parent species and their corresponding radical cations to further shed light onto the structural changes that take place upon oxidation.

EXPERIMENTAL SECTION

Full descriptions of all synthetic and electrochemical procedures, as well as details concerning instrumentation and digital simulation techniques, are provided in the Supporting Information.

RESULTS AND DISCUSSION

Synthesis and Characterization of PPh$_2$(dipp), 1, and PPh(dipp)$_2$, 2. Based on our previous experience with the synthesis of **3**,[8] we attempted the syntheses **1** and **2** from the corresponding chlorophenylphosphines, $PPh_{3-n}Cl_n$, by two routes: application of a standard Grignard method (dippMgBr/THF) and use of the aryl copper reagent, dipp$_4$Cu$_4$.[9] Use of the Grignard was the optimal approach for making **1** (Scheme 1A), as employment of dipp$_4$Cu$_4$ led

Scheme 1. Synthetic Routes to 1 (A) and 2 (B)

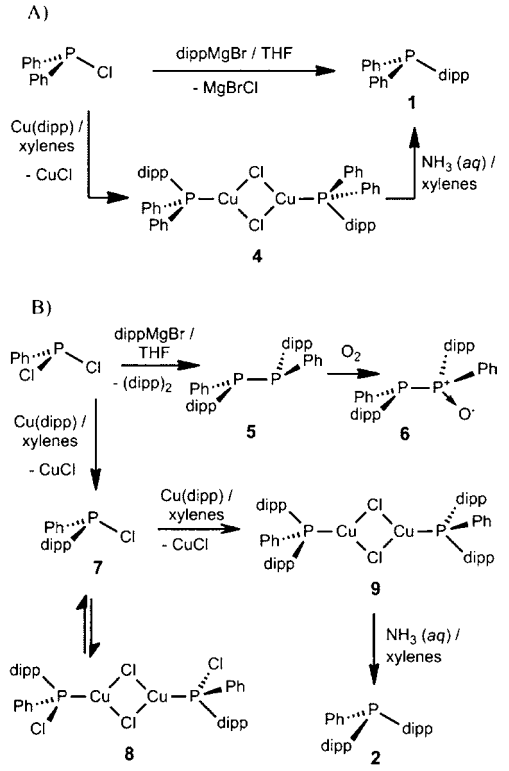

exclusively to the copper(I) chloride adduct **4** ($\delta(^{31}P)$ = −20.9 ppm, br s; see Supporting Information for additional characterization details and crystal structure description). This compound, in turn, yielded **1** via ammoniacal workup, albeit in low yield.

In contrast to the above, reaction of $PPhCl_2$ with 2 equiv of Grignard reagent did not yield **2** but, instead, the corresponding reductive coupling product, Ph(dipp)P-PPh(dipp), **5**, as the major product (Scheme 1B); similar coupling from the reduction of bulky Ar_2PCl species by organometallic reagents has previously been reported.[10] While ^{31}P NMR of **5** exhibits a singlet at −30.55 ppm, an attempted recrystallization from ethanol in air resulted in isolation of a new product exhibiting two doublets (δ = +39.43, −36.13 ppm, $^1J_{PP}$ = 279 Hz), which we ascribe to the monoxide Ph(dipp)P(O)PPh(dipp), **6**. We found that using the versatile dipp$_4$Cu$_4$ prevented the undesired reductive coupling and successfully yielded **2**, although certain aspects of the mechanism remain unclear. Specifically, we have previously shown that treatment of PCl_3 with dipp$_4$Cu$_4$ provides excellent yields of P(dipp)Cl$_2$,[9] but when dipp$_4$Cu$_4$ reacts with $PhPCl_2$, the major product, as determined by ^{31}P NMR studies of reaction aliquots, is [ClCuPPh(dipp)Cl]$_2$ (δ = 75.4 ppm, br s), **8**. Evidently the formation of **8** does not prevent the further substitution of the last chlorine on the phosphorus, but it is not clear whether that reaction happens while the chlorophosphine is coordinated to Cu(I) or whether reaction requires decomplexation, such that **8** acts only as a reservoir for the intermediate ClPPh(dipp). Furthermore, the final product of the aryl transfer reaction is another copper(I)

dx.doi.org/10.1021/ja403555d | J. Am. Chem. Soc. 2013, 135, 11205−11215

Table 1. Physical Properties and Characterization Data for PPh_3, 1, 2, 3, 10a−c, and 11a−c and DFT Structural Results for $PPh_3^{+\bullet}$, $1^{+\bullet}$, $2^{+\bullet}$, and $3^{+\bullet}$[a]

	base phosphine			
	PPh_3	**1**	**2**	**3**
$d(P-C)_{av}$,[b] Å	1.833(3)[g]	1.837(13)	1.854(14)	1.8507(16)[q]
P oop of 3 C_{ipso}'s,[b] Å	0.790[g]	0.739	0.651	0.539[q]
P oop of $C_{\neq ispo}$,[b] Å	0.071[g]	0.04−0.025	0.15−0.33	0.430[q]
$\sum\angle$(CPC),[b] deg	307.2[g]	314.7	324.6	335.6[q]
Stokes shift,[b] kJ·mol^{-1}	201[h]	183	146	129[q]
$\delta(^{31}P)$[b]	−4.7[i,j]	−20.9	−28.4	−49.7[q]
$\delta(^{31}P)$, E = O[c]	+29.6, +30.4[k]	+32.7	+31.2	
$\delta(^{31}P)$, E = S[d]	+41.7, +44.5[k]	+34.8	+31.2	
$\delta(^{31}P)$, E = Se[e]	+35.9, +36.5[i,k]	+25.2	+19.2	
$J(^{31}P-^{77}Se)$,[e] Hz	732[i]	734	690	
ν(P→O),[c] cm^{-1}	1190/1189[l]	1174/1175	1162/1162	
ν(P→S),[d] cm^{-1}	631[k]	610/610	603/603	
ν(P→Se),[e] cm^{-1}	558[k]	560/559	547/545	
$\sum\angle$(CPC)E=O,[c] deg	319.3[m]	322.4	328.0	
$\sum\angle$(CPC)E=S,[d] deg	317.6[n]	315.9	325.3	
$\sum\angle$(CPC)E=Se,[e] deg	318.2[o]	316.3	326.4	
$a_{iso}(^{31}P)$,[f] mT	29.9[p]		26.8	23.9[q]
$\sum\angle$(CPC)$R_3P^{+\bullet}$,[f] deg DFT	342.0	346.6	354.7	358.9[r]
$\sum\angle$(CPC)R_3P,[b] deg DFT	307.6	317.2	326.0	336.6
$\Delta\{\sum\angle(CPC)\}$,[b,c,d,e,f] deg DFT	34.4	29.4	28.7	22.3

[a]The source data for this table is located in the Supporting Information except where indicated. DFT performed at (r/u)b3lyp/6-31G(d,p) levels. [b]PR_3. [c]OPR_3. [d]SPR_3. [e]$SePR_3$. [f]$PR_3^{+\bullet}$. [g]Bruckmann, J.; Kruger, C.; Lutz, F. *Z. Naturforsch., B: Chem.Sci.* **1995**, *50*, 351. Kooijman, H.; Spek, A. L.; Bommel, K. J. C. van; Verboom, W.; Reinhoudt, D. N. *Acta Crystallogr., Sect. C: Cryst. Struct. Commun.* **1998**, *54*, 1695. [h]Changenet, P.; Plaza, P.; Martin, M. M.; Meyer, J. Y.; Rettig, W. *Chem. Phys.* **1997**, *221*, 311. [i]Allen, D. W.; Taylor, B. F. *J. Chem. Soc., Dalton Trans.*, **1982**, 51. [j]Schraml, J.; Čapka, M.; Blechta, V. *Magn. Reson. Chem.* **1992**, *30*, 544. [k]Chutia, P.; Kumari, N.; Sharma, M.; Woollins, J. D.; Slawin, A. M. Z.; Dutta, D. K. *Polyhedron* **2003**, *23*, 1657. [l]NIST Webbook: http://webbook.nist.gov/cgi/cbook.cgi?ID=C791286&Type=IR-SPEC&Index=1#IR-SPEC. [m]Brock, C. P.; Schweizer, W. B.; Dunitz, J. D. *J. Am. Chem. Soc.* **1985**, *107*, 6964. [n]C. R.de Arellano, G. Asensio, M. Medio-Simon, A. Cuenca, G. Mancha, private communication, 2007 (Cambridge Structural Database refcode: TPPOSS07). Schulz, T.; Meindl, K.; Leusser, D.; Stern, D.; Graf, J.; Michaelsen, C.; Ruf, M.; Sheldrick, G. M.; Stalke, D. *J. Appl. Crystallogr.* **2009**, *42*, 885. [o]Jones, P. G.; Kienitz, C.; Thone, C. *Z. Kristallogr.* **1994**, *209*, 80. A. L. Rheingold, private communication, 2011 (Cambridge Structural Database refcode: TPPHSE02). [p]Il'yasov, A. V.; Kargin, Yu. M.; Nikitin, E. V.; Vafina, A. A.; Romanov, G. V.; Parakin, O. V.; Kazakova, A. A.; Pudovik, A. N. *Phosphorus Sulfur* **1980**, *8*, 259. Il'yasov, A. V.; Kargin Yu. M.; Vafina, A. A. *Russ. J. Gen. Chem.*, **1993**, *63*,1833. [q]Boeré, R. T.; Bond, A. M.; Cronin, S.; Duffy, N. W.; Hazendonk, P.; Masuda, J. D.; Pollard, K.; Roemmele, T. L.; Tran, P.; Zhang, Y. *New J. Chem.* **2008**, *32*, 214. [r]360.0° reported by Pan, X.; Chen, X.; Li, T.; Li, Y.; Wang, X. *J. Am. Chem. Soc.*, **2013**, *135*, 3414.

complex, **9**, which we identified spectroscopically. Fortunately **9**, unlike **4**, affords free **2** in moderate yields upon treatment with deoxygenated aqueous ammonia followed by extraction into xylenes.

We characterized **1** and **2**, as well as their chalcogenide adducts (see below), by a variety of spectroscopic and physical methods (Table 1 and Supporting Information) and determined their structures in the solid state using single-crystal X-ray diffraction (Figure 1). Of particular importance is the degree of steric pressure and steric protection experienced in **1**, **2**, **3**, and PPh_3. Their respective $\sum\angle$(C−P−C) values show a systematic increase with number of dipp groups on the central phosphorus. As we have shown previously, the sums of angles around the P atom is a key parameter; substituents with sufficient steric bulk cause flattening at the central atom which raises the HOMO, thereby facilitating oxidation (vide infra).[8]

Various spectroscopic data indicate that the structural trends described above for the solid PPh_3 and **1**−**3** are also present in solution. For example, it has been shown that photoexcitation of phosphines involving promotion of a HOMO electron to an excited state induces a change to planar or close-to-planar geometries. Hence, the Stokes shift can be used to assess the effective pyramidalization of triarylphosphines in solution; large shifts, such as those reported for PPh_3, are observed when the ground state is highly pyramidal.[8,11,12] Stokes shifts of **1** and **2** (Table 1) are intermediate between those of PPh_3 and **3**. Similarly, ^{31}P NMR chemical shifts also change stepwise between those of PPh_3 and **3**. However, each of these measures shows a different degree of change with each added substituent, indicating that subtle structure−property effects are operative within the series.

Chemical Oxidation: Phosphine Chalcogenides 10a−c and 11a−c. In the syntheses of **1** and **2**, these compounds exhibited sensitivity toward atmospheric oxygen that is higher than either PPh_3 or **3**. In our previous work on **3**, we demonstrated its oxidation is induced strictly by electron transfer processes because the steric shielding by the exo isopropyl substituents blocks access of atom transfer reactions to the phosphorus atom.[8] PPh_3, in contrast, is easily accessible to oxidants but, as we discuss below, has a substantially higher oxidation potential. Thus **1** and **2** have lower steric protection than **3** and a more accessible oxidation potential than PPh_3. To further investigate this behavior, we systematically examined the chemical oxidation of **1** and **2** with oxygen, sulfur, and selenium. Both phosphines form thermally stable chalcogenides with oxygen (using H_2O_2 in acetone), yielding PPh_2(dipp)O, **10a**, and PPh(dipp)$_2$O, **11a**, as well as sulfur and selenium (by refluxing with the elements in xylenes), yielding PPh_2(dipp)S,

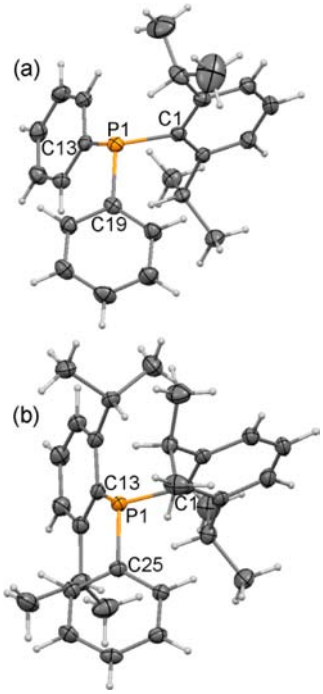

Figure 1. Thermal displacement plots (30% probability) of (a) **1** and (b) one of the independent molecules of **2** as determined in their crystal lattices. A symmetry code $(-x, 1-y, 1-z)$ was applied to the atom coordinates of **2** to emphasize the similarity in conformations of the two phosphines. For full atom numbers and the second molecule of **2** see the Supporting Information.

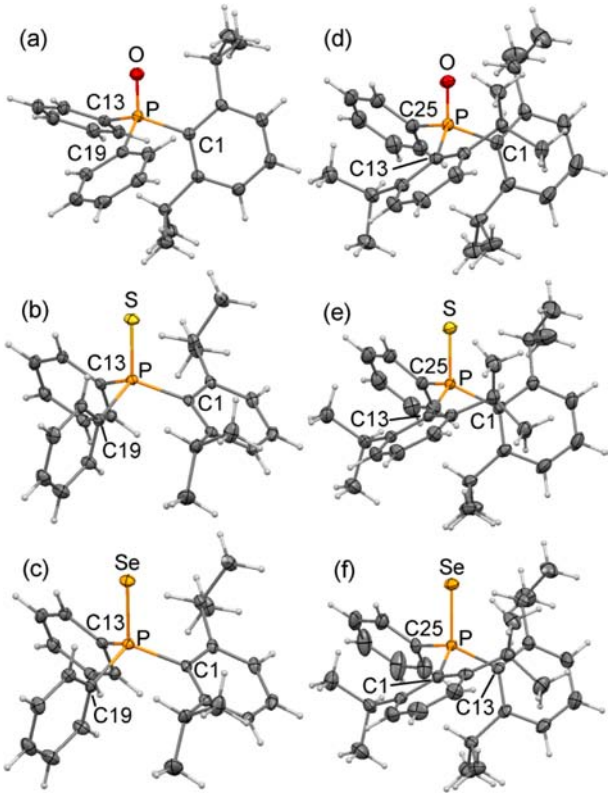

Figure 2. Thermal displacement plots (30% probability) of the structures of (a) **10a**, (b) **10b**, (c) **10c** (isostructural with **10b**), (d) **11a**, (e) **11b**, and (f) one of the independent molecules of **11c**, as determined in their crystal lattices. Symmetry codes were applied to the atom coordinates of **11b** $(1-x, 1-y, 1-z)$ and **11c** $(1/2+x, -y, 1/2+z)$ to emphasize the similarity in conformations among related phosphine chalcogenides. For full atom numbers and the second molecule of **11c** see the Supporting Information.

10b, $PPh_2(dipp)Se$, **10c**, $PPh(dipp)_2S$, **11b**, and $PPh(dipp)_2Se$, **11c**. We fully characterized all six derivatives and determined their structures by single-crystal X-ray crystallography (Figure 2). The solid-state structures show an increase in the steric flattening parameter $\sum\angle(CPC)$ upon oxidation, especially for the oxygen adducts. This is consistent with the formulation of $R_3P^+\rightarrow E^-$ for the bonding in the chalcogenides, which is strongly indicated in such oxides by solid state ^{17}O NMR spectroscopy.[13]

Room Temperature Electrochemical Studies. Cyclic voltammograms (19 ± 1 °C) of the oxidation of PPh_3 and compounds **1**–**3** in CH_2Cl_2 (0.5 M Bu_4NPF_6) at scan rates of 250 mV s^{-1} are presented in Figure 3. The results for PPh_3 are consistent with previously published accounts which indicated that the compound undergoes a diffusion-controlled but chemically irreversible one electron oxidation in organic solvents (eq 1).[14,15]

$$PPh_3 \rightarrow PPh_3^{+\cdot} + e^- \quad (1)$$

There is ample evidence that the electrogenerated phosphoniumyl radical cation, $PPh_3^{+\bullet}$, reacts rapidly with adventitious water in the solvent/electrolyte medium to ultimately yield the corresponding oxide, $OPPh_3$, and the hydrophosphonium cation, $HPPh_3^+$. If the concentration of water is high enough, the overall stoichiochiometry of the oxidation is described by eq 2, although published reports indicate that the product proportions will depend on the amount of water present in the reaction medium.

$$3PPh_3 + H_2O \rightarrow O{=}PPh_3 + 2HPPh_3^+ + 2e^- \quad (2)$$

The voltammograms in Figure 3 are consistent with one-electron oxidations of each of the triarylphosphines. In addition, they clearly illustrate that regular substitution of phenyl ligands with the sterically demanding dipp ligands results in an inductive effect, which shifts the oxidation peaks to lower potentials, and also bestows greater kinetic stability to the corresponding radical cations, as evidenced by enhanced

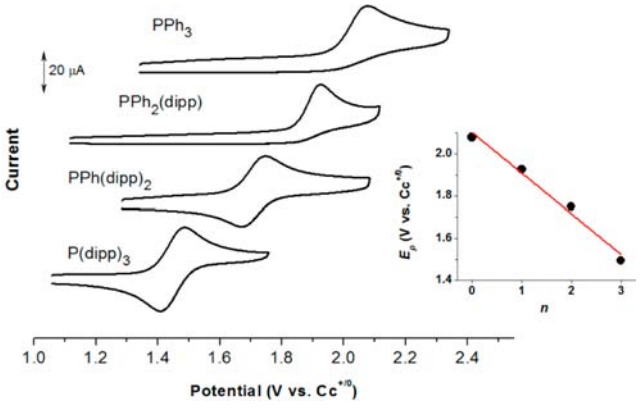

Figure 3. Cyclic voltammograms of compounds $PPh_{3-n}(dipp)_n$ in CH_2Cl_2 (0.5 M Bu_4NPF_6) at a 3 mm diameter GC electrode. The scan rate employed in all traces was 250 mV s^{-1}; analyte concentrations are between 0.8 and 1.0 mM. Inset: Oxidation peak potential as a function of the number of dipp ligands; the best linear fit (red line) has a slope of −190 mV per dipp substituent; peak potential measurements were reproducible to within 5 mV.

dx.doi.org/10.1021/ja403555d | J. Am. Chem. Soc. 2013, 135, 11205–11215

reversibility of the oxidation processes. These effects are summarized in Table 2 and are discussed in greater detail below.

Table 2. Summary of Room Temperature Electrochemical Data for the Oxidation of PPh_3, $P(mes)_3$, and Compounds 1−3 in CH_2Cl_2[a]

compound	E_p[b]	$E_{1/2}$[b]	i_r/i_f	k°[c]
PPh_3	2.078		0	0.10
$P(mes)_3$	1.579	1.547	0.88	0.063
1	1.926		0	0.081
2	1.748	1.710	0.77	0.031
3	1.487	1.449	0.97	0.067

[a]0.5 M Bu4NPF$_6$ electrolyte; GC working electrode; scan rate = 250 mV s^{-1}. [b]Oxidation peak potentials, E_p, and half-wave potentials, $E_{1/2}$, the average of the oxidation and reduction peak potentials for the reversible couple, are reported in V vs the $E_{1/2}$ of $Cc^{+/0}$. [c]Room temperature value of k°, in cm s^{-1}; estimated by optimizing digital simulations of ac voltammetric data.

The effect of steric crowding about the phosphorus center on the stabilities of triaryl phosphoniumyl cations has been the subject of previous work.[8,10,16−19] For example, the series $PPh_{3-n}(mes)_n$[16] exhibits similar trends to those observed in this work, with the oxidation of $P(mes)_3$ showing the greatest chemical reversibility. While oxidation of $P(mes)_3$ in our hands showed moderate chemical reversibility in dry, deoxygenated CH_2Cl_2 (i_r/i_f = 0.88 at 250 mV s^{-1}, where i_r/i_f is the ratio of the return to forward peak currents), the inertness of $\mathbf{3}^{+\bullet}$ afforded by the bulky isopropyl substituents makes the oxidation of the parent compound, **3**, even more chemically reversible (i_r/i_f = 0.97 at 250 mV s^{-1}). Similarly, the oxidation of **2** is coupled to a much larger cathodic return (i_r/i_f = 0.77 at 250 mV s^{-1}) than $P(mes)_2Ph$ (i_r/i_f = 0.17 at 5 V s^{-1}).[16] The relative inertness of $\mathbf{2}^{+\bullet}$ made it possible to characterize this species using EPR spectroelectrochemistry (Table 1 and Figure S11 in the Supporting Information). Interestingly, the previously reported reactivity of $P(mes)_3^{+\bullet}$ toward oxygen, which results in a virtually complete loss of peak reversibility and current attenuation by a factor of 0.5,[19] is shared by $\mathbf{2}^{+\bullet}$, but not $\mathbf{3}^{+\bullet}$. This observation, along with the peak current ratios mentioned above, implies that the accessibility of the phosphorus to chemical attack in $\mathbf{2}^{+\bullet}$ and $P(mes)_3^{+\bullet}$ is similar, i.e., the degree of steric protection afforded by three mesityl groups is comparable to that by the combination of one phenyl and two dipp ligands. This is consistent with the chemical oxidation studies reported above resulting in both **10a** and **11a**; similarly $P(mes)_3$ can form a stable oxide.[20] Finally, like PPh_3, electrooxidation of **1** is irreversible; apparently the steric protection afforded to the central phosphorus by a single dipp ligand is insufficient to protect it from rapid attack by adventitious water.

While the reversibility of the oxidation processes of $PPh_{3-n}(dipp)_n$ species makes qualitative comparisons of the relative stabilities of the corresponding radical cations straightforward, interpretation of the peak potentials is less so. The oxidation peak potentials, E_p, show an average shift of −190 mV per dipp ligand (Figure 3, inset), but exhibit a small deviation from linearity that we attribute to a number of effects. Specifically, the rapid homogeneous chemical processes coupled to the electron transfer for PPh_3 and **1** decrease the corresponding peak potentials from what would be observed for chemically reversible couples. Moreover, isopropyl groups in the ortho positions have both electronic and structural effects. Specifically, as the phosphorus becomes more congested, it is forced to assume a more planar geometry ($\sum\angle$(CPC) = 314.7°, 324.6°, and 335.6° for **1**, **2**, and **3**, respectively), resulting in a HOMO that becomes more 3p in character and higher in energy.[16,21] This decrease of pyramidalization is manifested in a correspondingly lower oxidation peak potential.

Electrochemical Mechanistic Studies. While there have been numerous reports on the electrochemical oxidation of PPh_3,[14,15,22] there is little rate information available on the rapid reactions coupled to the electrode process. Given the utility of such kinetic data to serve as a point of reference for the corresponding reaction rates of radical cations, $\mathbf{1}^{+\bullet}$, $\mathbf{2}^{+\bullet}$, and $\mathbf{3}^{+\bullet}$, we undertook a scan rate study of PPh_3 in CH_2Cl_2 (Figure 4).

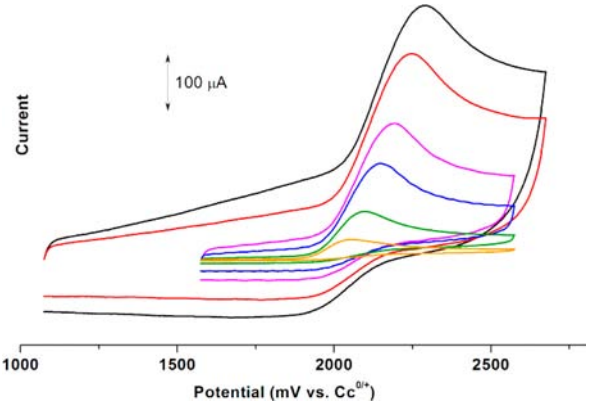

Figure 4. Dc voltammetric scan rate study of the oxidation of PPh_3 (2.6 mM) at a 3 mm glassy carbon electrode in CH_2Cl_2 (0.5 M Bu_4NPF_6); scan rates employed were 0.1 (orange), 0.5 (green), 2 (blue), 4 (magenta), 8 (red), and 12 V s^{-1} (black). Potentials are relative to the $Cc^{+/0}$ couple.

The voltammograms exhibited very little cathodic current coupled to the bulk oxidation at lower scan rates (ν < 2 V s^{-1}). Some return current is observed at higher scan rates, but the peak shapes are inconsistent with a simple EC mechanism. Rather, the elongation suggests that the first chemical step involves an equilibrium process that allows for the chemical regeneration of the reducible electrogenerated species during the reverse sweep.

To estimate the kinetic parameters of the coupled homogeneous reactions, we fit these voltammograms to the mechanism outlined in Scheme 2. This scheme, which is similar to that proposed for the attack of water on $P(mes)_3^{+\bullet}$ proposed by Gronchi and co-workers,[19] involves the radical abstraction of hydrogen from water by the phosphoniumyl cation, followed by attack of the resulting hydroxyl radical on a second electrogenerated phosphoniumyl cation. The final triarylphosphonium oxide is generated via rapid deprotonation by water; we did not consider a scheme involving deprotonation by the bulk phosphine, as previous work demonstrated that this process is slow on the cyclic voltammetry time scale.[22] Water concentrations from 0.5 to 2 mM were considered in the simulations, reasonable values given the routine steps taken in drying the solvent/electrolyte.

The observed peak shapes could be satisfactorily simulated by employing a relatively wide range of rate constants, with $k_{1,f}$ values ranging from about 1 × 10^6 M^{-1} s^{-1} up to the diffusion

dx.doi.org/10.1021/ja403555d | J. Am. Chem. Soc. 2013, 135, 11205−11215

Scheme 2. Generation and Reactivity of Triarylphosphoniumyl Cations (Ar = dipp or Ph)

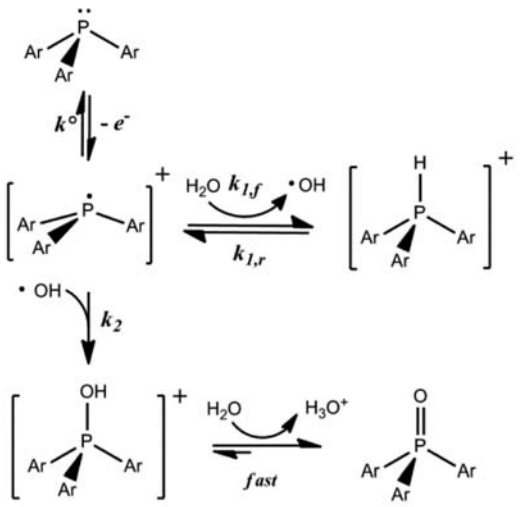

Room Temperature Rate Constants[a]

Parent Compound	$k_{1,f}$ (M^{-1} s^{-1})	$k_{1,r}$ (M^{-1} s^{-1})	k_2 (M^{-1} s^{-1})
PPh3	3×10^6	6×10^5	~1×10^8
1	8×10^5	1.5×10^5	~4×10^7
2	120	< 10	1×10^4
3	0	-	-

a. Additional parameters used in the simulations for these processes are provided in captions for Figures 5 and 8; the rate constant for the final deprotonation step was set at 1×10^8 M^{-1} s^{-1} in all simulations.

limit. The fitting is complicated by the large non-Faradaic currents that result from use of high scan rates with the macroelectrode. To get additional insight into the kinetics of the attack of water on $PPh_3^{+\bullet}$ we performed large amplitude Fourier-transformed ac voltammetry. This technique, which has been extensively employed by one of our laboratories in the investigation of a variety of electrode processes,[3,23−26] can provide reliable kinetic information on fast homogeneous coupled reactions without the use of microelectrodes.[25] By simultaneously fitting the current signals of all of the accessible harmonics of the forward and reverse sweeps of the voltammograms (Figure 5) we estimated $k_{1,f}$ (3×10^6 M^{-1} s^{-1}) more precisely than was possible from the dc voltammetric results. Other optimized simulation parameters are provided in Scheme 2 and the caption of Figure 5. Because several of the kinetic and electron transfer parameters can compensate for one another in the ac voltammetry simulations, we found that simulations of similar quality could be obtained using $k_{1,f}$ values between 1×10^6 and 1×10^7 M^{-1} s^{-1} and standard rate constant, $k°$, values between 0.08 and 0.15 cm s^{-1}. For comparison, this places $k°$ in a range comparable to that which we found for the oxidation of ferrocene using similar techniques.[26]

Large amplitude ac voltammetric experiments were also performed on compounds **1**−**3** to measure their $k°$ values and the reaction rates of their respective radical cations at ambient temperature. Fit optimization of the resulting voltammograms (vide infra) yielded the kinetic parameters shown in Scheme 2.

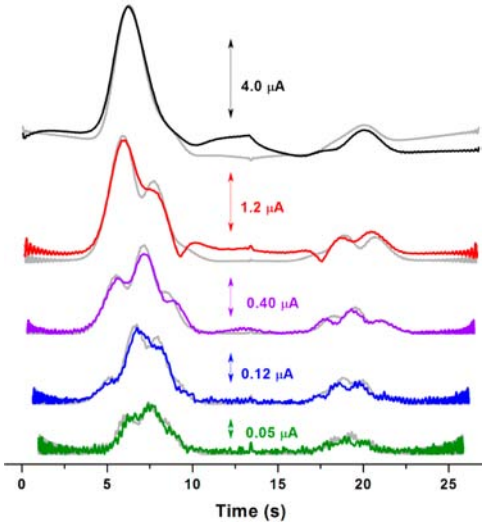

Figure 5. Experimental (colored) and digital simulations (gray) of the second (black), third (red), fourth (violet), fifth (blue), and sixth (green) harmonics of room temperature ac voltammograms of the oxidation of 1.0 mM PPh_3 in CH_2Cl_2. Experimental parameters: f = 14.16 Hz, ΔE = 100 mV, ν = 59.60 mV s^{-1}, T = 19 °C, A = 0.047 cm^2; the switch time for the potential sweep direction is at 13.4 s. Simulation parameters: R_u = 200 Ω, $k°$ = 0.1 cm s^{-1}, α = 0.5, diffusion coefficients for all species except water, $D = 1.5 \times 10^{-5}$ cm^2 s^{-1}, $D_{H_2O} = 2.2 \times 10^{-5}$ cm^2 s^{-1}, C_{DL} constants: E_c = 1.6 V, $c_0 = 1.8 \times 10^{-4}$ F cm^{-2}, $c_1 = 1.8 \times 10^{-5}$ F cm^{-2} V^{-1}, $c_2 = -1.4 \times 10^{-5}$ F cm^{-2} V^{-2}.

We discuss these results briefly below. As previously mentioned, substitution of one phenyl ligand with a dipp ligand does not appreciably affect the reversibility of the bulk oxidation. The optimized rate constants for the reaction of $1^{+\bullet}$ with residual water are slightly lower than those for PPh_3, but appear to be within an order of magnitude. The $k°$ values are also similar. In contrast, the corresponding rate constant for $2^{+\bullet}$ decreases by more than 3 orders of magnitude compared to $1^{+\bullet}$. While we used the same operative mechanism to fit the voltammogram of **2**, it is worth noting that equally good fits could be obtained by a simple EC mechanism owing to the slow rates of the reactions following the initial attack by water. Furthermore, the heterogeneous rate constant for the oxidation of **2** is somewhat lower than those of the other compounds in the series, a characteristic that has a significant effect on its low temperature ac voltammetric response, as discussed more fully below. Finally, $3^{+\bullet}$ is unreactive toward adventitious water on the time scale of these experiments.[8]

Effect of Temperature on Dc and Ac Voltammetry. Previous studies of **3** in our laboratories indicated that this compound, despite its chemically reversible oxidation, undergoes electron transfer slowly enough for the anodic process to be considered only quasi-reversible.[8] It therefore falls in a kinetic regime that makes fundamental studies concerning the mechanism of its electron-transfer attractive using FT ac voltammetry. The determination of electron-transfer activation parameters using dc cyclic voltammetry is usually difficult because the temperature changes that affect the electrode kinetics also affect solution resistance and diffusion coefficients. We have shown, however, that large amplitude ac techniques are ideal for distinguishing and quantifying these effects.[23,24b,c] In our previous work using this technique to measure the activation parameters of electrode processes we focused on highly chemically reversible couples of metallocenes;[26] the

dx.doi.org/10.1021/ja403555d | J. Am. Chem. Soc. 2013, 135, 11205−11215

current work demonstrates the approach can be applied more generally, that is to systems with various degrees of chemical irreversibility.

To illustrate how the ac and dc techniques differ with respect to their temperature responses, we present in Figure 6 a comparison of voltammograms of the oxidation of, from top to bottom, $P(mes)_3$, **3**, **2**, and **1**, obtained by the two methods over a roughly 40 °C range; for the sake of clarity, only the fourth harmonic of each ac voltammogram is presented, but others show similar effects as can be seen in Figures 7 and 8. $P(mes)_3$ is included in these analyses because its electrode kinetics and activation energy are similar in some ways to that of ferrocene and therefore serves as a useful comparison for the other systems. What is particularly noteworthy of the voltammograms in Figure 6 is the fact that, uniformly, temperature has relatively small effects on the dc response but shows a larger effect on the ac data, significantly so in some cases. This sensitivity to temperature in the ac data enables the estimation of the relevant standard rate constants as illustrated below.

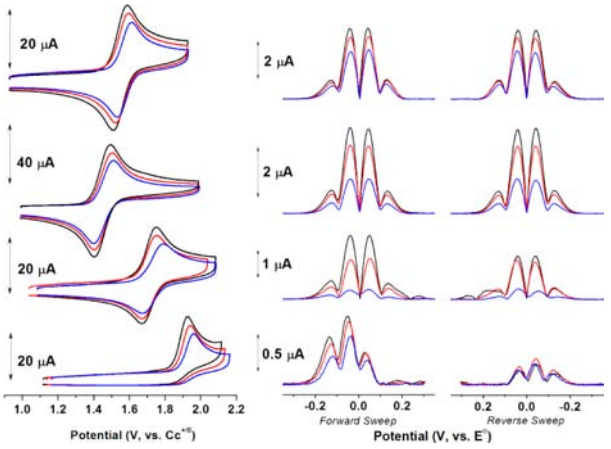

Figure 6. Dc (left) and ac (right columns, fourth harmonic only) voltammograms obtained for CH_2Cl_2 solutions of, from top, $P(mes)_3$ (0.9 mM), **3** (1.7 and 0.6 mM in dc and ac experiments, respectively), **2** (0.8 mM), and **1** (0.9 mM) at 19 ± 1 °C (black), 1 ± 1 °C (red), and −19 ± 1 °C (blue). Scan rates were 250 mV s^{-1} in all dc experiments; in ac experiments scan rates between 60 and 75 mV s^{-1} were used with ΔE = 100 mV and f = 14 ± 0.3 Hz. Potentials for the ac data are relative to the $E°$ of the analyte as estimated from iterative fitting (see text).

As temperature is lowered, the dc voltammograms of $P(mes)_3$ show only a slight decrease in current, owing to a decrease in the diffusion coefficient, and a small shift in $E_{1/2}$ value relative to the $Cc^{0/+}$ internal standard. Little discernible effect attributable to slower electron transfer kinetics or increased solution resistance is observed. This stands in contrast to the more significant changes seen in the ac voltammograms due to increases in uncompensated resistance, R_u and decreases in $k°$ which result from the lowered temperatures. Note that the two envelopes of peaks in the ac voltammograms correspond to the forward and reverse sweeps of the cycle; in the cases of $P(mes)_3$ and **3** the two sets of peaks are very similar in shape and size as would be expected for a chemically reversible couple. By simultaneously fitting all of the available harmonics obtained at each temperature (Figures 7 and 8), relatively precise estimates of R_u and $k°$ values are obtained. Moreover, because fitting the data requires diffusion coefficients, we performed double-potential step chronocoulometry experiments at each temperature and used Anson plots, Q vs $t^{1/2}$, to obtain those values.[27] With respect to the

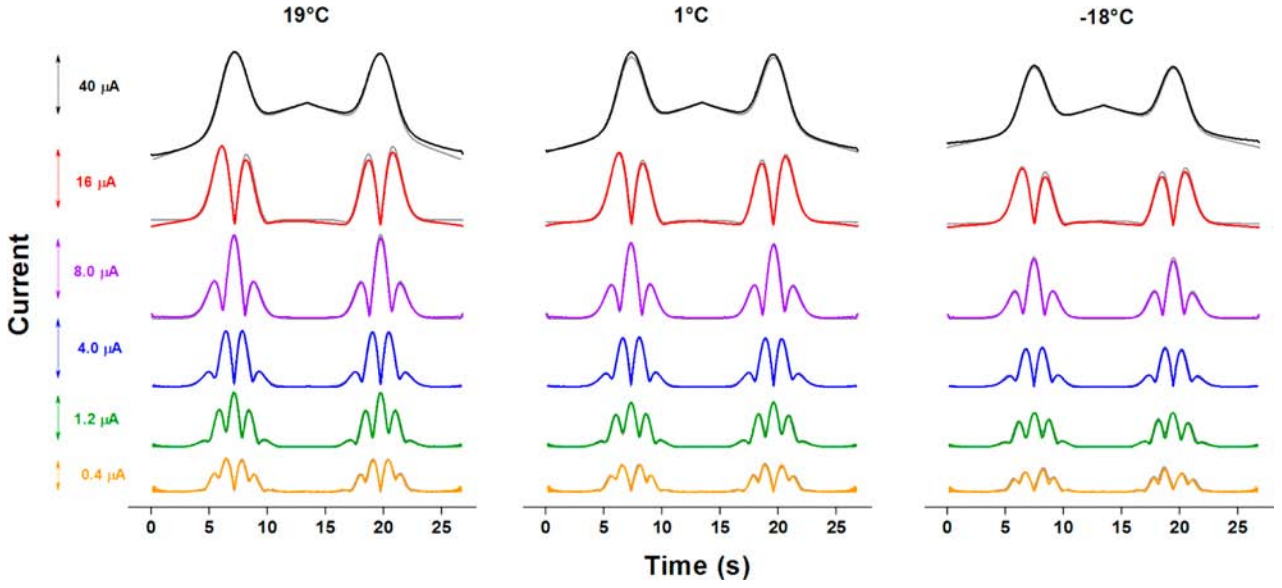

Figure 7. Experimental (colored) and digital simulations (gray) of the fundamental (black), second (red), third (violet), fourth (blue), fifth (green), and sixth (orange) harmonics of ac voltammograms of the oxidation of 0.86 mM $P(mes)_3$ in CH_2Cl_2 obtained at 19°, 1°, and −18 °C. Experimental parameters: f = 13.78 Hz, ΔE = 100 mV, ν = 59.60 mV s^{-1}, A = 0.050 cm^2; the switch time for the potential sweep direction is at 13.4 s. Optimized simulation parameters employed at each temperature are listed: (**19 °C**) R_u = 175 Ω, $k°$ = 0.063 cm s^{-1}, α = 0.48, D = 1.13 × 10^{-5} cm^2 s^{-1}; C_{DL} constants, E_c = 0.9 V, c_0 = 1.26 × 10^{-4} F cm^{-2}, c_1 = 5.8 × 10^{-5} F cm^{-2} V^{-1}, c_2 = 2 × 10^{-6} F cm^{-2} V^{-2}; (**1 °C**) R_u = 225 Ω, $k°$ = 0.048 cm s^{-1}, α = 0.46, D = 0.97 × 10^{-5} cm^2 s^{-1}; C_{DL} constants, E_c = 0.7 V, c_0 = 9.4 × 10^{-5} F cm^{-2}, c_1 = 5.0 × 10^{-5} F cm^{-2} V^{-1}, c_2 = 6 × 10^{-6} F cm^{-2} V^{-2}; (**−18 °C**) R_u = 300 Ω, $k°$ = 0.031 cm s^{-1}, α = 0.44, D = 0.68 × 10^{-5} cm^2 s^{-1}; C_{DL} constants, E_c = 0.7 V, c_0 = 7.0 × 10^{-5} F cm^{-2}, c_1 = 4.4 × 10^{-5} F cm^{-2} V^{-1}, c_2 = 9 × 10^{-6} F cm^{-2} V^{-2}.

dx.doi.org/10.1021/ja403555d | J. Am. Chem. Soc. 2013, 135, 11205−11215

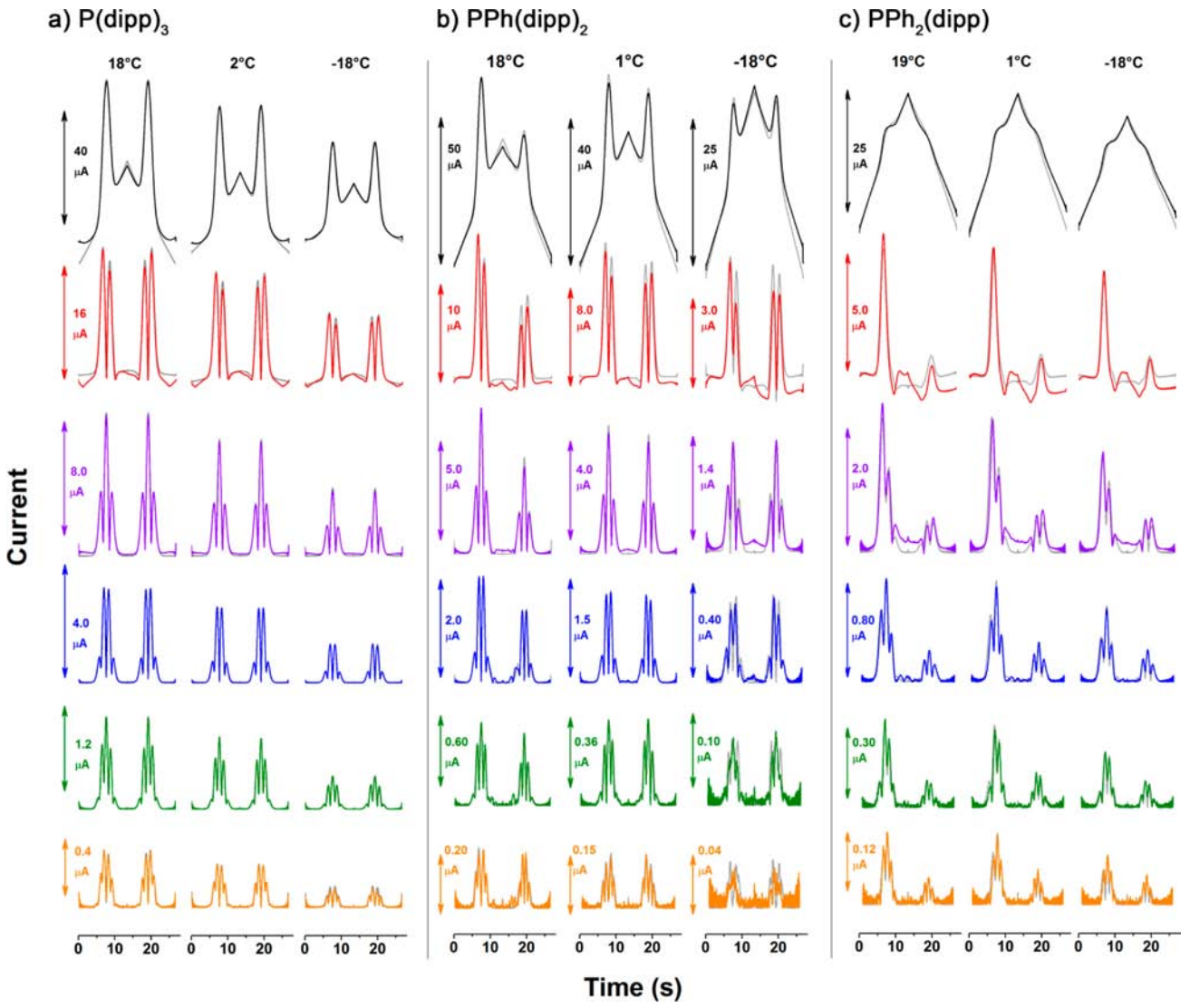

Figure 8. Experimental (colored) and digital simulations (gray) of, from top to bottom, the fundamental through sixth harmonics of ac voltammograms of the oxidation of (a) 0.62 mM **3**, (b) of 0.80 mM **2**, and (c) 0.90 mM **1**, all in CH_2Cl_2 (0.5 M Bu_4NPF_6), at the temperatures indicated. Specific experimental and optimization parameters: (a) f = 14.31 Hz, ΔE = 100 mV, ν = 67.06 mV s^{-1}, electrode area = 0.057 cm^2; switch time for the potential sweep direction is 13.4 s. Optimized simulation parameters employed at each temperature: (**18 °C**) R_u = 200 Ω, $k°$ = 0.076 cm s^{-1}, α = 0.50, $D_{O,R}$ = 1.35 × 10^{-5} cm^2 s^{-1}, C_{DL} constants, E_c = 0.8 V, c_0 = 9.5 × 10^{-5} F cm^{-2}, c_1 = 4.6 × 10^{-5} F cm^{-2} V^{-1}, c_2 = 6 × 10^{-6} F cm^{-2} V^{-2}; (**2 °C**) R_u = 275 Ω, $k°$ = 0.036 cm s^{-1}, α = 0.49, $D_{O,R}$ = 1.02 × 10^{-5} cm^2 s^{-1}; C_{DL} constants, E_c = 0.8 V, c_0 = 7.8 × 10^{-5} F cm^{-2}, c_1 = 4.2 × 10^{-5} F cm^{-2} V^{-1}, c_2 = 1.2 × 10^{-5} F cm^{-2} V^{-2}; (**−18 °C**) R_u = 290 Ω, $k°$ = 0.0148 cm s^{-1}, α = 0.485, $D_{O,R}$ = 0.75 × 10^{-5} cm^2 s^{-1}; C_{DL} constants, E_c = 0.2 V, c_0 = 3.6 × 10^{-5} F cm^{-2}, c_1 = 1.2 × 10^{-5} F cm^{-2} V^{-1}, c_2 = 1.2 × 10^{-6} F cm^{-2} V^{-2}. (b) f = 14.04 Hz, ΔE = 100 mV, ν = 74.51 mV s^{-1}, electrode area = 0.047 cm^2; switch time for the potential sweep direction is 13.4 s. Optimized simulation parameters employed at each temperature: (**18 °C**) R_u = 180 Ω, $k°$ = 0.031 cm s^{-1}, α = 0.50, $D_{O,R}$ = 1.50 × 10^{-5} cm^2 s^{-1}, [H_2O] = 0.7 mM, D_{H_2O} = 2.2 × 10^{-5} cm^2 s^{-1}, $k_{C1,f}$ = 120 M^{-1} s^{-1}, $k_{C1,r}$ = 1 M^{-1} s^{-1}, k_{C2} = 1 × 10^4 M^{-1} s^{-1}; C_{DL} constants, E_c = 0.8 V, c_0 = 1.17 × 10^{-4} F cm^{-2}, c_1 = 5.4 × 10^{-5} F cm^{-2} V^{-1}, c_2 = 0 F cm^{-2} V^{-2}; (**1 °C**) R_u = 225 Ω, $k°$ = 0.0175 cm s^{-1}, α = 0.47, $D_{O,R}$ = 1.15 × 10^{-5} cm^2 s^{-1}, [H_2O] = 0.7 mM, D_{H_2O} = 1.4 × 10^{-5} cm^2 s^{-1}, $k_{C1,f}$ = 15 M^{-1} s^{-1}, $k_{C1,r}$ = 1 M^{-1} s^{-1}, k_{C2} = 1 × 10^4 $M^{-1}s^{-1}$; C_{DL} constants, E_c = 0.8 V, c_0 = 1.00 × 10^{-4} F cm^{-2}, c_1 = 4.7 × 10^{-5} F cm^{-2} V^{-1}, c_2 = 0 F cm^{-2} V^{-2}; (**−18 °C**) R_u = 650 Ω, $k°$ = 0.0076 cm s^{-1}, α = 0.47, $D_{O,R}$ = 0.75 × 10^{-5} cm^2 s^{-1}, [H_2O] = 0.7 mM, D_{H_2O} = 1.0 × 10^{-5} cm^2 s^{-1}, $k_{C1,f}$ = 0 M^{-1} s^{-1}; C_{DL} constants, E_c = 0.8 V, c_0 = 9.1 × 10^{-5} F cm^{-2}, c_1 = 4.3 × 10^{-5} F cm^{-2} V^{-1}, c_2 = 5.0 × 10^{-5} F cm^{-2} V^{-2}. (c) f = 14.16 Hz, ΔE = 100 mV, ν = 59.60 mV s^{-1}, electrode area = 0.045 cm^2; switch time for the potential sweep direction is 13.4 s. Optimized simulation parameters employed at each temperature: (**19 °C**) R_u = 180 Ω, $k°$ = 0.081 cm s^{-1}, α = 0.50, $D_{O,R}$ = 1.2 × 10^{-5} cm^2 s^{-1}, [H_2O] = 0.7 mM, D_{H_2O} = 2.2 × 10^{-5} cm^2 s^{-1}; C_{DL} constants, E_c = 1.0 V, c_0 = 1.48 × 10^{-4} F cm^{-2}, c_1 = 4.3 × 10^{-5} F cm^{-2} V^{-1}, c_2 = −6 × 10^{-6} F cm^{-2} V^{-2}; (**1 °C**) R_u = 220 Ω, $k°$ = 0.054 cm s^{-1}, α = 0.50, $D_{O,R}$ = 9 × 10^{-6} cm^2 s^{-1}, [H_2O] = 0.7 mM, D_{H_2O} = 1.4 × 10^{-5} cm^2 s^{-1}; C_{DL} constants, E_c = 1.0 V, c_0 = 1.36 × 10^{-4} F cm^{-2}, c_1 = 4.5 × 10^{-5} F cm^{-2} V^{-1}, c_2 = −2 × 10^{-6} F cm^{-2} V^{-2}; (**−18 °C**) R_u = 300 Ω, $k°$ = 0.028 cm s^{-1}, α = 0.50, $D_{O,R}$ = 6.5 × 10^{-6} cm^2 s^{-1}, [H_2O] = 0.7 mM, D_{H_2O} = 1.0 × 10^{-5} cm^2 s^{-1}; C_{DL} constants, E_c = 1.0 V, c_0 = 1.28 × 10^{-4} F cm^{-2}, c_1 = 3.8 × 10^{-5} F cm^{-2} V^{-1}, c_2 = −3 × 10^{-6} F cm^{-2} V^{-2}.

uncertainties for the $k°$ values, they are considerably smaller than that for PPh_3 owing to the lack of coupled chemistry and the correspondingly smaller number of input parameters involved in fitting the data. We estimate optimized values of $k°$ for $P(mes)_3$, **2**, and **3** are correct to within about 10%; those for **1** are somewhat larger, about ±25%.

dx.doi.org/10.1021/ja403555d | J. Am. Chem. Soc. 2013, 135, 11205−11215

Given the relatively small effects of temperature on the dc voltammograms in Figure 6, the range of effects on the ac data is remarkable. Oxidation of **3** is similar to that of $P(mes)_3$ in terms of its chemical reversibility, but the current attenuation at lower temperatures is more pronounced, reflecting a greater temperature dependence of the heterogeneous kinetics. An even more dramatic decrease in oxidative current is seen for **2**. In addition, the lower reaction rate of $\mathbf{2}^{+\bullet}$ toward water at lower temperatures largely compensates for the slower electrode kinetics so that the current maxima of the return sweeps observed at 18 and 1 °C are nearly equivalent. Finally, the chemical irreversibility of the oxidation of **1** has the effect of significantly distorting the peak shapes[25] and diminishing all of the currents compared to those of the other systems shown. Given the relatively small differences in the fourth harmonic responses for the oxidation of **1**, it would be difficult, on the basis of this harmonic alone, to distinguish the effect of temperature on diffusion characteristics, solution resistance, and electrode and chemical kinetics. Fortunately, since the ac experiment yields numerous harmonics simultaneously, each of which differs in its response to these various effects,[24a,25,26] it is possible to estimate these parameters with greater precision than the data in Figure 6 would suggest.

Determination of Electron Transfer Activation Parameters. We used the standard rate constants obtained by the fit optimizations presented in Figure 7 for the oxidation of $P(mes)_3$ to estimate the activation energy, E_{act}, of the electrode process at the glassy carbon electrode by means of an Arrhenius plot (Figure 9a); the data show good linearity, and the resulting slope yields an activation energy of 12 kJ mol^{-1}. As explained below, this value is very close to the outer sphere component of the electron transfer activation energy according to Marcus–Hush theory, suggesting that the inner sphere component, i.e., the energetic barrier to bond length and other structural changes, is quite small. For comparison, the inner sphere component for the oxidation of ferrocene is estimated to be about 0.6 kJ mol^{-1}.[28]

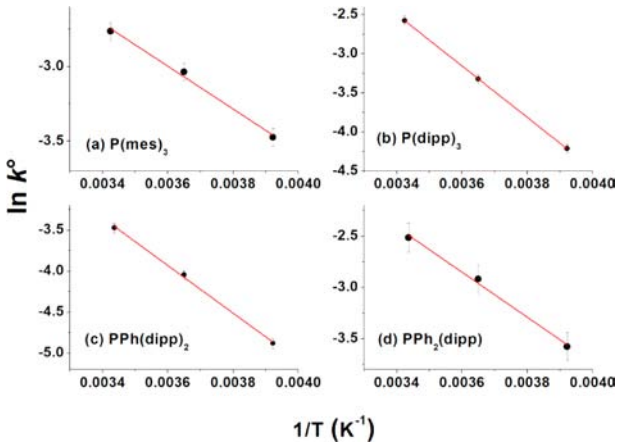

Figure 9. Arrhenius plots and linear fits of the standard rate constants for (a) $P(mes)_3$, (b) **3**, $P(dipp)_3$, (c) **2**, $PPh(dipp)_2$, and (d) **1**, $PPh_2(dipp)$; error bars indicate the estimated uncertainties for the rate constants.

The activation energy for any electron transfer process is the sum of the inner and outer sphere components (eq 3). The outer sphere component can be calculated using eq 4,[29] where N is the Avogadro constant, e is the charge on the electron, ε_0, $\varepsilon_{op,r}$, and $\varepsilon_{s,r}$, are the permittivity of free space, the relative permittivity of the solvent at optical frequencies, and the corresponding relative static permittivity, respectively. The temperature dependence of the latter two terms has been shown to be small and is neglected in the following analysis.[30] The terms r_A and r_e are the radius of the reactive species and the imaging distance to the electrode, usually assumed to be infinity.[31] We employed the following constants[28] in eq 4: for dichloromethane, $\varepsilon_{op,r} = 2.03$, and $\varepsilon_{s,r} = 9.0$, and for $P(mes)_3$, $r_A = 0.54$ nm;[32] a theoretical value, $\Delta G^{\ddagger}_{os} = 12.2$ kJ mol^{-1}, is thereby obtained.

$$\Delta G^{\ddagger}_{ET} = \Delta G^{\ddagger}_{is} + \Delta G^{\ddagger}_{os} \tag{3}$$

$$\Delta G^{\ddagger}_{os} = \frac{Ne^2}{32\pi\varepsilon_0}\left(\frac{1}{r_A} - \frac{1}{r_e}\right)\left(\frac{1}{\varepsilon_{op,r}} - \frac{1}{\varepsilon_{s,r}}\right) \tag{4}$$

The close agreement between the experimentally determined E_{act} value and the calculated value of $\Delta G^{\ddagger}_{os}$ for $P(mes)_3$ stands in contrast to the results we obtained for the dipp-substituted compounds. Figure 8a–c shows the fundamental through sixth harmonics of the Fourier transformed ac voltammograms for compounds **3**, **2**, and **1**, respectively, at temperatures similar to those employed in the examination of $P(mes)_3$. As mentioned above, $P(mes)_3$ and **3** show similar voltammetric characteristics except that the ac currents of the latter are considerably smaller at lower temperatures. Simulations of the data reveal that this difference is due to a greater temperature sensitivity of $k°$ for **3**. The resulting Arrhenius plot of the best fit $k°$ values (Figure 9b) yields an activation barrier of 25 kJ mol^{-1}. This compares to a calculated value of $\Delta G^{\ddagger}_{os}$ of only 11.4 kJ mol^{-1} (obtained using an average radius of 0.58 nm[8]). The inner sphere component of the barrier to electron transfer must therefore be much higher for **3** than $P(mes)_3$. We attribute this to the greater steric congestion afforded by the ortho substituents of the dipp ligand relative to those of mesityl. We return to this point after discussing Arrhenius analyses of the oxidation of **2** and **1**, below.

The $k°$ values obtained for **2** and **1** yielded activation energies of 24 and 18 kJ mol^{-1}, respectively (Figures 9c and 9d). The corresponding calculated values of $\Delta G^{\ddagger}_{os}$ are only 11.8 and 13.0 kJ mol^{-1}. As was the case with PPh_3, the estimates of $k°$ values for **1** are less precise owing to the rapid coupled chemistry. While the uncertainty warrants more caution in the interpretation of this plot (Figure 9d), it appears the presence of even just one dipp ligand introduces a significant barrier to electron transfer beyond that expected for a simple outer sphere process. Furthermore, some comment on the unusually large current diminution for **2** compared to **3** warrants mention. While such a contrast in temperature response may seem incongruous with the similar activation barriers we find for these compounds, the $k°$ values of **2** are in a kinetic regime in which the higher harmonic currents are particularly sensitive to changes in the heterogeneous rate constants.[26] Thus, what appears to be a "collapse" of the current at lower temperatures, especially in the higher harmonics in this data series, is not due to a larger activation barrier but, instead, is a result of the consistently lower values of $k°$ across this temperature series relative to those of **3**. We also note that the dc voltammogram for **2** at −18° (Figure 6, third row, left) is unique in that series as it is the only one in which the value of $k°$ becomes small enough to make the peak

dx.doi.org/10.1021/ja403555d | J. Am. Chem. Soc. 2013, 135, 11205–11215

separation noticeably larger than those obtained at higher temperatures.

In contrast to $P(mes)_3$, E_{act} values for the oxidation of **1**, **2**, and **3** are all substantially larger than their respective outer sphere components as calculated by eq 4. To aid in the interpretation of these observations, we performed a series of DFT calculations to determine the structural changes that should take place upon oxidation of these compounds (Table 1). All of the compounds should "flatten" to some extent, a process that could involve considerable rearrangement of the intermeshing isopropyl substituents for the $\mathbf{3}^{0/+}$ couple, but relatively little of the methyl groups in the less congested $P(mes)_3^{0/+}$ system. The flattening, expressed as the increase in $\sum\angle(CPC)$ upon oxidation, was calculated to be 38.5°, 28.7°, and 22.2° for **1**, **2**, and **3**, respectively (Table 1), and 23.9° for $P(mes)_3$. The smaller degree of flattening calculated for $P(mes)_3^+$ and $\mathbf{3}^{+\bullet}$ is a result of the steric congestion of the parent compounds, i.e., these compounds start out flatter in their reduced forms and so undergo less dramatic changes in pyramidalization when oxidized. The very small $\Delta G^{\ddagger}_{is}$ for the oxidation of $P(mes)_3$ that our results imply indicates that ortho methyl groups on adjacent aryl rings undergo a minimum of steric intermeshing upon flattening of the molecule. The situation is dramatically different for triarylphosphines with bulky ortho substituents. Our activation data indicate that $\Delta G^{\ddagger}_{is}$ is actually lowest for **1** and increases with increased dipp substitution, despite the calculated decrease of flattening that occurs upon oxidation across the series. A reasonable explanation for this unexpected trend is that the greatest contribution to inner sphere reorganization is not the magnitude of flattening per se, but rather the intermeshing of the ortho isopropyl groups with neighboring substituents; the size of this effect for the redox couples is $\mathbf{3}^{0/+} > \mathbf{2}^{0/+} > \mathbf{1}^{0/+}$ (space filling views of the structures are provided in Figure S3 in the Supporting Information to illustrate these interactions). Hence the apparent similarity in the total steric crowding of the central phosphorus atoms of **2** and $P(mes)_3$, reflected by the aforementioned similar i_r/i_f ratios of the dc voltammograms, does not result in similar activation profiles because the total steric congestion does not reflect regions of locally greater steric interactions that can inhibit structural reorganization and, thereby, affect the kinetics of the electron transfer.

These results represent the first systematic investigation of sterics on heterogeneous electron transfer across any homologous series. While there is no reason to anticipate that this is not a more general phenomenon, its relevance to the chemistry of congested phosphines is particularly acute. Unexpected consequences of sterically demanding substituents in phosphorus chemistry have been recognized previously from structural and reactivity studies.[6] To the best of our knowledge, our work is the first to detect such effects from activation energies of redox reactions.

CONCLUSION

In this work we describe the synthesis and characterization of a series of triarylphosphines that spans the limits of the steric possibilities of this class of compounds. All members of the series undergo one-electron oxidation processes, the potentials of which exhibit a pronounced induction effect. The kinetic stabilities of the resulting radical cations depend on the steric congestion about the central phosphorus; more congested compounds are resistant to attack by adventitious water, while those with more accessible phosphorus centers react rapidly. Digital simulations of the dc and ac voltammograms are consistent with a radical mechanism involving abstraction of hydrogen from water. In addition to the above effects, the presence of dipp ligands also has a pronounced effect on the activation barrier to electrooxidation, an effect we attribute to the unique energetics associated with conformational changes of the phosphines upon oxidation that result from the extreme crowding from the ortho isopropyl substituents. The greater reactivity of **1** and **2** compared to both PPh_3 and **3** has been confirmed through chemical synthesis of chalcogenides **10a–c** and **11a–c**.

ASSOCIATED CONTENT

Supporting Information

Crystallographic data in electronic (CIF) format. Synthetic procedures and spectroscopic characterization (^1H, ^{13}C, and ^{31}P NMR, UV–vis, IR, Raman, fluorescence) of compounds **1**, **2**, **4**, **9**, **10a–c**, and **11a–c**. Details of the crystal structure determinations with selected interatomic distances for **1**, **2**, **4**, **10a–c**, and **11a–c**. Tables and assignments of vibrational (FTIR and FT-Raman), electronic, and fluorescence peaks. Spectroelectrochemical EPR characterization of $\mathbf{2}^{+\bullet}$. Minimized geometries determined in the DFT calculations. This material is available free of charge via the Internet at http://pubs.acs.org.

AUTHOR INFORMATION

Corresponding Author

jbullock@bennington.edu; boere@uleth.ca, alan.bond@monash.edu

Notes

The authors declare no competing financial interest.

ACKNOWLEDGMENTS

R.T.B. thanks the Natural Sciences and Engineering Research Council of Canada, the University of Lethbridge, and the Canada Foundation for Innovation for operating and equipment funding. Dr. M. Gerken is thanked for the use of his FT-Raman instrument. The financial support of the Australian Research Council is gratefully acknowledged.

REFERENCES

(1) The following are seminal papers concerning the role of sterics in a range of reaction types: (a) Dostrovsky, I.; Hughes, E. D.; Ingold, C. K. *J. Chem. Soc.* **1946**, 173–194. (b) Basolo, F.; Chatt, J.; Gray, H. B.; Pearson, R. G.; Shaw, B. L. *J. Chem. Soc.* **1961**, 2207–2215. (c) Brown, H. C.; Sclesinger, H. I.; Cardon, S. Z. *J. Am. Chem. Soc.* **1942**, *64*, 325–329. (d) Griller, D.; Ingold, K. U. *Acc. Chem. Res.* **1976**, *9*, 13–19.

(2) Hubig, S. M.; Rathore, R.; Kochi, J. K. *J. Am. Chem. Soc.* **1999**, *121*, 617–626.

(3) Bond, A. M.; Duffy, N. W.; Guo, S.-X.; Zhang, J.; Elton, D. M. *Anal. Chem.* **2005**, *77*, 186A–195A.

(4) (a) Fischer, R. C.; Power, P. P. *Chem. Rev.* **2010**, *110*, 3877–3923. (b) Power, P. P. *Chem. Rev.* **1999**, *99*, 3463–3503. (c) Li, L.; Fukawa, T.; Matsuo, T.; Hashizume, D.; Fueno, H.; Tanaka, K.; Tamao, K. *Nat. Chem.* **2012**, *4*, 361–365. (d) Power, P. P. *Nat. Chem.* **2012**, *4*, 343–344. (e) Wang, Y.; Quillian, B.; Wei, P.; Wannere, C. S.; Xie, Y.; King, R. B.; Schaefer, H. F.; Schleyer, P. V.; Robinson, G. H. *J. Am. Chem. Soc.* **2007**, *129*, 12412–12413. (f) Wang, Y. Z.; Xie, Y. M.; Wei, P. R.; King, R. B.; Schaefer, H. F.; Schleyer, P. V.; Robinson, G. H. *Science* **2008**, *321*, 1069–1071. (g) Wang, Y. Z.; Xie, Y. M.; Wei, P. R.; King, R. B.; Schaefer, H. F.; Schleyer, P. V.; Robinson, G. H. *J. Am. Chem. Soc.* **2008**, *130*, 14970–14971. (h) Kinjo, R.; Donnadieu, B.; Celik, M. A.; Frenking, G.; Bertrand, G. *Science* **2011**, *333*, 610–613. (i) Valente, C.; Calimsiz, S.; Hoi, K. H.; Mallik, D.; Sayah, M.; Organ,

M. G. *Angew. Chem., Int. Ed.* **2012**, *51*, 3314−3332. (j) Balogh, J.; Slawin, A. M. Z.; Nolan, S. P. *Organometallics* **2012**, *31*, 3259−3263. (k) Rekken, B. D.; Brown, T. M.; Fettinger, J. C.; Tuononen, H. M.; Power, P. P. *J. Am. Chem. Soc.* **2012**, *134*, 6504−6507. (l) Summerscales, O. T.; Olmstead, M. M.; Power, P. P. *Organometallics* **2011**, *30*, 3468−3471. (m) Woodul, W. D.; Carter, E.; Müller, R.; Richards, A. F.; Stasch, A.; Kaupp, M.; Murphy, D. M.; Driess, M.; Jones, C. *J. Am. Chem. Soc.* **2011**, *133*, 10074−10077;. (n) Sheberla, D.; Tumanskii, B.; Bravo-Zhivotovskii, D.; Molev, G.; Molev, V.; Lee, V. Y.; Takanashi, K.; Sekiguchi, A.; Apeloig, Y. *Organometallics* **2010**, *29*, 5596-−5606;. (o) Ishida, S.; Hirakawa, F.; Iwamoto, T. *J. Am. Chem. Soc.* **2011**, *133*, 12968−12971..

(5) (a) Pan, X.; Chen, X.; Li, T.; Li, Y.; Wang, X. *J. Am. Chem. Soc.* **2013**, *135*, 3414−3417. (b) Pan, X.; Su, Y.; Chen, X.; Li, Y.; Zuo, J.; Wang, X. *J. Am. Chem. Soc.* **2013**, *135*, 5561−5564.

(6) (a) Protasiewicz, J. D.; Washington, M. P.; Gudimetla, V. B.; Payton, J. L.; Simpson, M. C. *Inorg. Chim. Acta* **2010**, *364*, 39−45. (b) Dutan, C.; Shah, S.; Smith, R. C.; Choua, S.; Berclaz, T.; Geoffroy, M.; Protasiewicz, J. D. *Inorg. Chem.* **2003**, *42*, 6241−6251. (c) Smith, R. C.; Gleason, L. B.; Protasiewicz, J. D. *J. Mater. Chem.* **2006**, *16*, 2445−2452. (d) Smith, R. C.; Ren, T.; Protasiewicz, J. D. *Eur. J. Inorg. Chem.* **2002**, 2779−2783. (e) Smith, R. C.; Shah, S.; Urnezius, E.; Protasiewicz, J. D. *J. Am. Chem. Soc.* **2003**, *125*, 40−41.

(7) (a) Stephan, D. W. *Org. Biomol. Chem.* **2008**, *6*, 1535−1539. (b) Stephan, D. W.; Erker, G. *Angew. Chem., Int. Ed.* **2010**, *49*, 46−76. (c) Ménard, G.; Hatnean, J. A.; Cowley, H. J.; Lough, A. J.; Rawson, J. M.; Stephan, D. W. *J. Am. Chem. Soc.* **2013**, *135*, 6446−6449.

(8) Boeré, R. T.; Bond, A. M.; Cronin, S.; Duffy, N. W.; Hazendonk, P.; Masuda, J. D.; Pollard, K.; Roemmele, T. L.; Tran, P.; Zhang, Y. *New J. Chem.* **2008**, *32*, 214−231.

(9) Boeré, R. T.; Masuda, J. D.; Tran, P. *J. Organomet. Chem.* **2006**, *691*, 5585−5591.

(10) Sasaki, S.; Yoshifuji, M. *Curr. Org. Chem* **2007**, *11*, 17−31.

(11) Changenet, P.; Plaza, P.; Martin, M. M.; Meyer, J. Y.; Rettig, W. *Chem. Phys.* **1997**, *221*, 311−322.

(12) Rozanel'skaya, N. A.; Bokanov, A. I.; Uzhinov, B. M.; Stepanov, B. I. *J. Gen. Chem. USSR* **1975**, *45*, 277−280.

(13) Bryce, D. L.; Eichele, K.; Wasylishen, R. E. *Inorg. Chem.* **2003**, *42*, 5085−5096.

(14) Schiavon, G.; Zercchin, S.; Cogoni, G.; Bontempelli, G. *J. Electroanal. Chem.* **1973**, *48*, 425−431.

(15) Ohmori, H.; Nakai, S.; Masui, M. *J. Chem. Soc., Perkin Trans. 1* **1978**, 1333−1335.

(16) Culcasi, M.; Berchadsky, Y.; Gronchi, G.; Tordo, P. *J. Org. Chem.* **1991**, *56*, 3537−3542.

(17) Tordo, P. In *The Chemistry of Organophosphorus Compounds*; Hartley, F. R., Ed., Wiley: Chichester, 1990; Vol. *1*, Chapter 6.

(18) (a) Sasaki, S.; Sutoh, K.; Murakami, M.; Yoshifuji, M. *J. Am. Chem. Soc.* **2002**, *124*, 14830−14831. (b) Sasaki, S.; Chowdhury, R.; Yoshifuji, M. *Tetrahedron Lett.* **2004**, *45*, 9193−9196.

(19) Merzougui, B.; Berchadsky, Y.; Tordo, P.; Gronchi, G. *Electrochim. Acta* **1997**, *42*, 2445−2453.

(20) Zagumennov, V. A.; Nikitin, E. V. *Russ. J. Electrochem.* **2003**, *39*, 1236−1239.

(21) Palau, C.; Berchadsky, Y.; Chalier, F.; Finet, J.-P.; Gronchi, G.; Tordo, P. *J. Phys. Chem.* **1995**, *99*, 158−163.

(22) Caram, J. A.; Vasini, E. J. *Electrochim. Acta* **1994**, *39*, 2395−2400.

(23) Bond, A. M.; Duffy, N. W.; Elton, D. M.; Fleming, B. D. *Anal. Chem.* **2009**, *81*, 8801−8808.

(24) (a) Zhang, J.; Guo, S.-X.; Bond, A. M. *Anal. Chem.* **2007**, *79*, 2276−2288. (b) Sher, A. A.; Bond, A. M.; Gavaghan, D. J.; Harriman, K.; Feldberg, S. W.; Duffy, N. W.; Guo, S.-X.; Zhang. *J. Anal. Chem.* **2004**, *76*, 6214−6228. (c) Zhang, J.; Guo, S.-X.; Bond, A. M. *Anal. Chem.* **2007**, *79*, 2276−2288. (d) O'Mullane, A. P.; Zhang, J.; Brajter-Toth, A.; Bond, A. M. *Anal. Chem.* **2008**, *80*, 4614−4626. (e) Guo, S.; Zhang, J.; Elton, D. M.; Bond, A. M. *Anal. Chem.* **2004**, *76*, 166−177. (f) Fleming, B. D.; Barlow, N. L.; Zhang, J.; Bond, A. M.; Armstrong, F. A. *Anal. Chem.* **2006**, *78*, 2948−2956. (g) Lee, C. Y.; Fleming, B. D.; Zhang, J.; Guo, S.-X.; Elton, D. M.; Bond, A. M. *Anal. Chim. Acta* **2009**, *652*, 205−214. (h) Fleming, B. D.; Zhang, J.; Elton, D. M.; Bond, A. M. *Anal. Chem.* **2007**, *79*, 6516−6526. (i) Lertanantawong, B.; O'Mullane, A. P.; Zhang, J.; Surareungchai, W.; Somasudrum, M.; Bond, A. M. *Anal. Chem.* **2008**, *80*, 6515−6525.

(25) Lee, C.-Y.; Bullock, J. P.; Kennedy, G. F.; Bond, A. M. *J. Phys. Chem. A* **2010**, *114*, 10122−10134.

(26) Bullock, J. P.; Mashkina, E.; Bond, A. M. *J. Phys. Chem. A* **2011**, *115*, 6493−6502.

(27) Bard, A. J.; Faulkner, L. R. *Electrochemical Methods: Fundamentals and Applications*, 2nd ed.; Wiley: New York, 2001; Chapter 5.

(28) Gennett, T.; Milner, D. F.; Weaver, M. J. *J. Phys. Chem.* **1985**, *89*, 2787−2794.

(29) Marcus, R. A. *J. Chem. Phys.* **1965**, *43*, 679−701.

(30) Richardson, J. N.; Harvey, J.; Murray, R. W. *J. Phys. Chem.* **1994**, *98*, 13396−13402.

(31) Fawcett, W. R.; Opallo, M. *Angew. Chem., Int. Ed. Engl.* **1994**, *33*, 2131−2143.

(32) The value for the average molecular radius is calculated from X-ray crystallographic data by treating the molecules as oblate spheres and using the van der Waals surface at points of greatest separation. For $P(mes)_3$, dimensions of 14.1 and 7.3 Å were used. See: Bott, R. C.; Bowmaker, G. A.; Buckley, R. W.; Healy, P. C.; Perera, M. C. S. *Aust. J. Chem.* **2000**, *53*, 175−181. Blount, J. F.; Camp, D.; Hart, R. D.; Healy, P. C.; Skelton, B. W.; White, A. H. *Aust. J. Chem.* **1994**, *47*, 1631−1639.